LAWRENCE
LIVERMORE
NATIONAL
LABORATORY

LLNL-JRNL-634412

Hall Anomaly and Quantum Oscillations of Surface States in Bi0.91Sb0.09 (111)

D. Qu, S. K. Roberts, G. F. Chapline

April 10, 2013

Physical Review Letters

Disclaimer

Hall Anomaly and Quantum Oscillations of Surface States in $Bi_{0.91}Sb_{0.09}$ (111)

Dong-Xia Qu[1], Sarah K. Roberts, and George F. Chapline[1]
[1]*Lawrence Livermore National Laboratory, Livermore, CA 94550, USA*
(Dated: April 8, 2013)

We report the observation of low field Hall anomaly and quantum oscillations arising from surface states in topological insulator $Bi_{0.91}Sb_{0.09}$ (111). The temperature-dependent resistivity profile shows a thermal activation behavior with an activation gap of 11 meV. We find that, in spite of strong disorder caused by alloying, the holelike surface currents with a mobility 23 000-85 000 cm^2/V s can be directly uncovered in the Hall signal. In a magnetic field up to 31 Tesla, we observed pronounced quantum oscillations coming from a two-dimensional Fermi surface. The Fermi velocity of 1×10^5 m/s obtained from Shubnikov-de Haas oscillations is consistent with the value of holelike surface state observed in angle-resolved photoemission experiments.

PACS numbers: 73.20.At, 73.25.+i, 71.18.+y, 75.47.-m

Electronic systems with spin-polarized relativistic carriers are promising candidates for spintronic and quantum information processing applications. One mechanism to realize a spin-split system is the Rashba effect, which removes the spin degeneracy as a result of spin-orbit interaction and inversion symmetry breaking. This effect is especially prominent in bismuth-based materials, including bismuth (Bi) single crystals [1–3], Bi/Ag(111) surface alloys [4], Bi/Si(111) semiconductor systems [5], and BiTeI bulk crystals [6]. Recently, the discovery of unusual surface states in topological insulator $Bi_{1-x}Sb_x$ has attracted huge interest [7–14]. This alloy has a complex surface band structure with chiral spin textures, as revealed by angle-resolved photoemission spectroscopy (ARPES) [15–18] and scanning tunnelling microscope (STM) experiments [19]. Finding the transport information of these surface states is a key factor to evaluate whether or not they are suitable for future device applications. However, to date low-field magnetotransport [20, 21] and magneto-optical [22] measurements have concentrated on surface states on the $(2\bar{1}\bar{1})$ surface of $Bi_{1-x}Sb_x$. Little research on the transport properties of the surface states on the (111) surface was implemented.

In this letter, we show the presence of holelike surface states in $Bi_{0.91}Sb_{0.09}$ (111) from the weak-field Hall effect and Shubnikov-de Haas (SdH) oscillations. At low H, we observe a huge Hall anomaly, revealing the high surface mobility μ = 23 000 - 80 000 cm^2/V s. The magnitude of the Hall anomaly is consistent with the carrier density determined from the SdH oscillations. By titling the field relative to the trigonal axis, we find that the quantum oscillations originate from a two-dimensional (2D) Fermi surface. In addition, the holelike surface conduction accounts for $\sim$ 10% of the total conduction in a macroscopic crystal.

The surface electronic structure of insulating $Bi_{1-x}Sb_x$ (111) was directly identified by ARPES measurements. Fig. 1(a) shows the Fermi surface map in the first Brillouin zone, which consists of an electron pocket enclosing the $\overline{\Gamma}$ point, six hole pockets in between $\overline{\Gamma}$ and $\overline{\mathrm{M}}$,

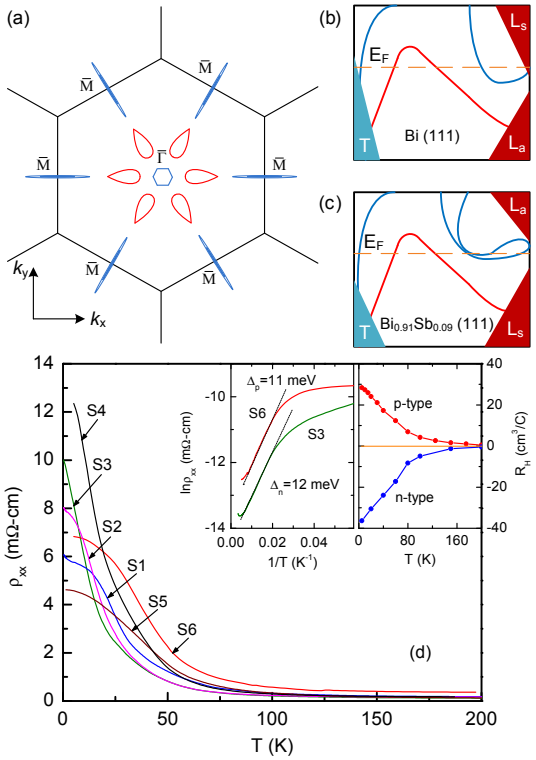

FIG. 1: (a) Sketch of the (111) surface Brillouin zone with a hexagonal electron pocket around $\overline{\Gamma}$, six tear-shaped hole pockets along the $\overline{\Gamma} - \overline{\mathrm{M}}$ direction, and six bowtie-shaped electron pockets around $\overline{\mathrm{M}}$. (b)-(c) Surface band structure along the $\overline{\Gamma} - \overline{\mathrm{M}}$ direction mapped by ARPES experiments in (b) Bi (111) [16] and (c) $Bi_{0.91}Sb_{0.09}$ (111) [17]. (d) The ρ_{xx} vs T for samples $S1$-$S6$ between 4 and 200 K. The left panel of the insets shows the Arrhenius plot of $\ln\rho_{xx}$ vs $1/T$ for n-type sample $S3$ and p-type sample $S6$. The right panel shows Hall coefficient R_H vs T for representative n- and p-type samples.

and six electron pockets near the $\overline{\mathrm{M}}$ point. As shown in Fig. 1(b) and 1(c), the existence of degenerate electron pockets close to $\overline{\mathrm{M}}$ is sensitive to the Sb substitution at $x = 0.07$ (the topological phase transition point), whereas the spin-splitting electron and hole pockets surrounding the $\overline{\Gamma}$ point are robust against Sb variation

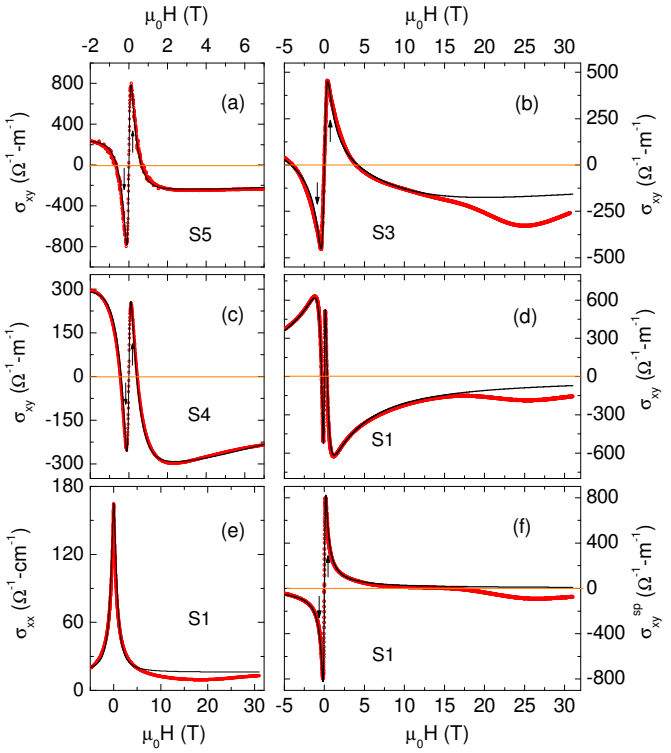

FIG. 2: (a)-(d) The Hall conductivity σ_{xy} vs H for samples $S5$, $S3$, $S4$, and $S1$ (red circles). The solid line is the fit to σ_{xy} in Eq. (1). Arrows indicate the peak field B_p, which is related to mobility by $\mu_{sp} = 1/B_p$. (e) The conductivity σ_{xx} measured with H at 0.3 K for sample $S1$ (red circles). The solid curve is the calculated σ_{xx} from Eq. (1) with a bulk mobility $\mu_b = 13\ 000$ cm^2/V s. (f) The holelike surface Hall conductivity σ^{sp}_{xy} vs H, obtained by subtracting the bulk term σ^b_{xy} and electronlike surface Hall conductivity σ^{sn}_{xy} at $T = 0.3$ K for sample $S1$. The solid curve is the fit to Eq. (2).

[16]. STM measurements discovered that the backscattering between these spin-polarized surface states is significantly suppressed [19].

Single crystals $Bi_{1-x}Sb_x$ studied here were grown by modified Bridgman method [23]. The samples were cleaved along the trigonal (111) plane without forming micrometer scale terraces on top and bottom surfaces. For $x = 0.09$, the Fermi level is inside the bulk band gap and the crystals display an insulating behavior. As shown in Fig. 1 (d), the resistivity ρ_{xx} in samples $S1$-$S6$ steeply increases by almost two orders of magnitude when temperature T is lowered from 200 to 4 K. The Hall resistivity ρ_{yx} in $S1$-$S5$ is n-type, whereas ρ_{yx} in $S6$ is p-type. The Arrhenius plot of ρ_{xx} in samples $S1$ and $S6$ indicates a thermal activation behavior with an activation gap $\Delta = 12$ and 11 meV, respectively. Moreover, the Hall coefficient R_H in n- and p- type samples exhibits similar magnitudes [Fig. 1(d), inset], which suggests that the electron and hole bulk conduction are comparable and compensated.

The pronounced weak-field Hall anomaly is resolved in n-type samples. In Figs. 2(a)-2(e), we plot the observed Hall conductivity σ_{xy} (red dots) in five different samples $S1$-$S5$. For these samples the applied H can change σ_{xy} from holelike to electronlike at fields below 1 Tesla. This dispersive anomaly dominates the low field Hall conduction in accordance with a high mobility band that is p-type. This effect is similar to what has been found in topological insulator Bi_2Te_3, where a n-type Hall anomaly is observed in a p-type crystal and is confirmed to originate from topological surface states [24].

TABLE I: Parameters in samples $S1$, $S2$, $S3$, $S4$, and $S5$. The dimension of the sample $L \times W \times t$ (length, width, thickness) is in unit of μm. The uncertainties in measuring t is approximately $\pm 10\%$. μ_{sp} and n_{sp} correspond to the Hall mobility and carrier density of the holelike surface state, respectively. S_F, k_F, and $k_F l$ are the Fermi surface cross section, average wavevector, and metallicity parameter of the p-type surface state, respectively. All these values are obtained from fitting measured $\sigma_{xy}(H)$ and $\sigma_{xx}(H)$ to Eq. (1) at 0.3 K.

Units	$L \times W \times t$ μm^3	μ_{sp} m^2/V s	n_{sp} 10^{12}cm^{-2}	S_F T	k_F (Å^{-1})	$k_F l$ -
$S1$	$825 \times 170 \times 30$	6.0	5.30	18.3	0.024	220
$S2$	$350 \times 170 \times 20$	8.0	1.80	6.21	0.013	95
$S3$	$880 \times 390 \times 40$	2.3	10.8	37.3	0.034	162
$S4$	$600 \times 300 \times 30$	8.0	1.48	5.10	0.012	75
$S5$	$840 \times 270 \times 50$	8.5	6.28	21.7	0.026	368

To quantitatively understand the anomalous Hall signal, we fit the observed Hall conductivity as the sum of three conductivity tensors

$$\sigma_{ij} = \sigma^b_{ij} + \sigma^{sp}_{ij} + \sigma^{sn}_{ij} \quad (1)$$

where σ^b_{ij} is the bulk conductivity, σ^{sp}_{ij} the p-type surface conductivity, and σ^{sn}_{xy} the n-type surface conductivity. With $\sigma^s_{ij} = G^s_{ij}/t$ (t is the sample thickness), G^s_{xy} corresponds to the surface Hall conductance, given by

$$G^s_{xy} = g_i \frac{2\pi e^3}{h^2} \frac{Bl^2}{[1 + (\mu B)^2]} \quad (2)$$

where g_i is the degeneracy of the surface band i ($g_i = 6$ for the holelike band), l the mean free path, h Planck's constant, e the electron charge, and μ the surface Hall mobility, which is related to the metallicity parameter $k_F l$ as $\mu = el/\hbar k_F$.

We can achieve a very close fit to the observed conductivity σ_{xx} and Hall conductivity σ_{xy} by Eqs. (1) and (2) in four different samples at low H [solid lines, Figs. 2(a)-2(d)]. In Fig. 2(f), the calculated p-type surface term in $S1$ is plotted in solid curve, which well captures the profile of isolated surface conductivity, red circles, obtained by subtracting $\sigma^b_{xy} + \sigma^{sn}_{xy}$ from the observed σ_{xy}. We find that G^s_{xy} reaches the maximum value $G^{\max}_{xy} = (e^2/2h) g_i k_F l$ at the peak field $B_p = 1/\mu$ [black arrows in Fig. 2]. Thus the H-dependent G^s_{xy} profile

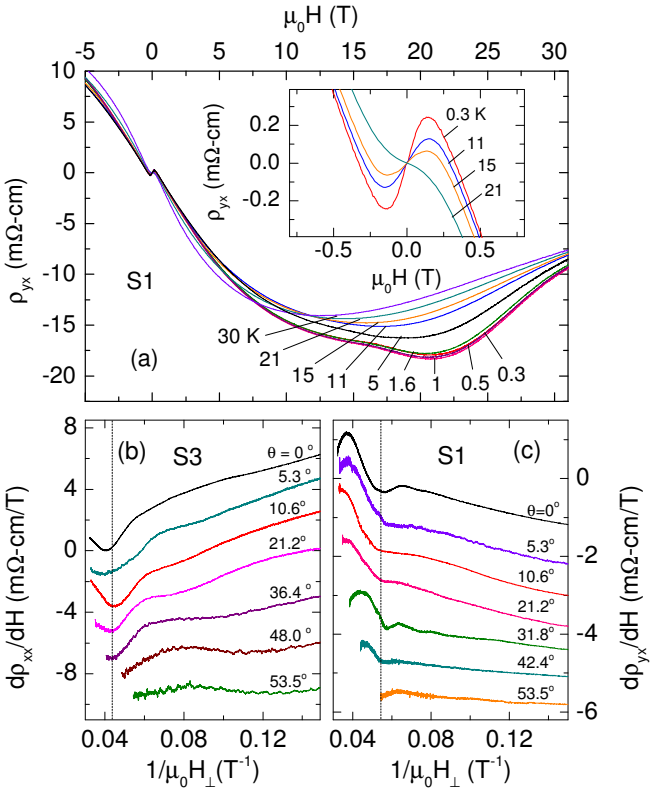

FIG. 3: (a) The trace of Hall resistivity ρ_{yx} vs H in sample $S1$ measured at temperature T between 0.3 and 30 K. The inset shows that the amplitude of weak-field Hall anomaly decreases rapidly as T is raised from 0.3 to 21 K. (b) The resistivity derivative $d\rho_{xx}/dH$ vs $1/H_\perp$ with $H_\perp = H\cos\theta$ at selected tilt angles θ in sample $S3$. (c) The Hall resistivity derivative $d\rho_{yx}/dH$ vs $1/H_\perp$ at various θ in sample $S1$.

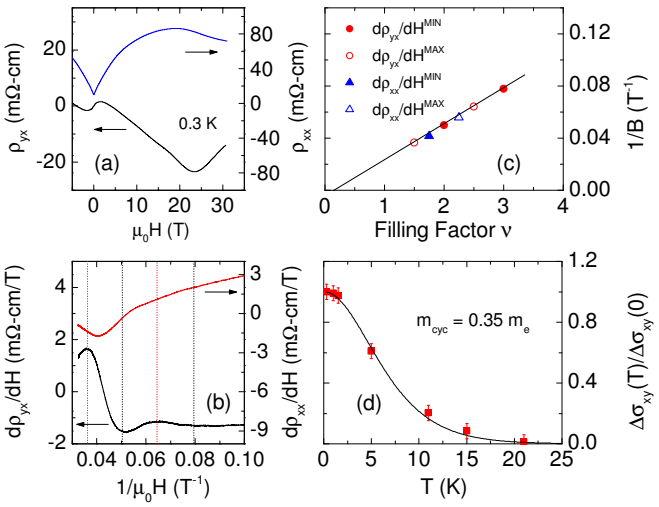

FIG. 4: (a) ρ_{xx} and ρ_{yx} vs H in sample $S3$ at 0.3 K. (b) The high-field quantum oscillations in the plot of $d\rho_{xx}/dH$ and $d\rho_{yx}/dH$ vs $1/H$. Black and red dashed lines correspond to the minima and maxima of $d\rho_{yx}/dH$, which are phase shifted by $\pi/2$ from the extrema of $d\rho_{xx}/dH$. (c) The Landau level index plot using the extrema of $d\rho_{xx}/dH$ and $d\rho_{yx}/dH$. (d) The normalized Hall conductivity amplitude $\Delta\sigma_{xy}(H)/\Delta\sigma_{xy}(0)$ vs T at 0.3 K with 15 T. The fit to the Lifshitz-Kosevich expression gives $m_{cyc} = 0.35m_e$.

provides a good estimation of the mobility and carrier density for the surface hole pockets. Table I summarizes the parameters for five samples that all display a weak-H Hall anomaly. The extracted surface hole band mobility is in the range of 23 000 to 85 000 cm^2/V s.

The bulk band mobility μ_b may be estimated from the transverse magnetoresistance, as the reduction in $\sigma_{xx}(H)$ is predominantly determined by μ_b via $\sigma_{xx}(H) = \sigma_{xx}(0)/[1 + (\mu_b H)^2]$. For sample $S1$ [Fig. 2(e)], the reduction in σ_{xx} by 79% at 2 T yields $\mu_b \sim 10\,000$ cm^2/V s, consistent with the identified n-type high mobility state from Hall analysis. We note that both the n- and p-type crystals exhibit a thermal activation behavior with a similar transport band gap [Fig. 1(d)]. This implies that the electron and hole bulk bands are highly compensated. Fitting $\sigma_{xx}(H)$ along with $\sigma_{xy}(H)$ yield the bulk p and n type carrier density $n_b = 3.48, 2.72 \times 10^{16}$ cm^{-3}, respectively, and surface electron density $n_{sn} = 2.5 \times 10^{13}$ cm^{-2} with $\mu_{sn} = 3000$ cm^2/V s.

If we associate a spherical Fermi surface to the bulk carriers, these carrier concentrations set the quantum limit at a magnetic field $B_{\nu=1} = S_F/(2\pi)^2\phi_0$, where ν is the filling factor, $\phi_0 = h/e$ the magnetic flux quanta, and S_F the extremal cross section of the Fermi surface. For samples $S1$ and $S3$, we calculate $B_{\nu=1} = 3.36$ and 2.81 T, respectively, for bulk electrons, and $B_{\nu=1} = 2.85$ and 2.78 T, respectively, for bulk holes. Previous studies on $Bi_{0.91}Sb_{0.09}$ also identified that the bulk quantum limit is attained by a field $H \leq 3$ T [21].

We next report the detection of quantum oscillations in the resistivity tensors at a tilting magnetic field up to 31 T, which is far above the ultraquantum limit of bulk carriers. As shown in Fig. 3(a), the raw trace of Hall resistivity, ρ_{yx}, displays weakly resolved oscillations, sitting on top of a strongly nonlinear background for fields exceeding 10 T. As T is raised from 0.3 to 21 K, the oscillation amplitudes decrease quickly, accompanied by the decrease of the Hall anomaly [inset of Fig. 3(a)]. Figs. 3(b) and 3(c) plot the derivative $d\rho_{xx}/dH$ and $d\rho_{yx}/dH$ versus the perpendicular field component $H_\perp = H\cos\theta$ along the trigonal axis [111] (θ is the tilting field relative to the trigonal axis), for samples $S3$ and $S1$, respectively. For both samples, the most pronounced dip (marked by dashed lines) depends only on $H_\perp$, and they are absent for $55° \leq \theta \leq 90°$. This distinct feature is a direct evidence of the surface origin of the high-H quantum oscillations.

Figure 4(a) shows the traces of $\rho_{yx}(H)$ and $\rho_{xx}(H)$ versus H for sample $S3$ at 0.3 K. We find that the quantum oscillations are more prominent in $\rho_{yx}(H)$ than in $\rho_{xx}(H)$. This observation may be understood by taking

account of the huge magnetoresistance arising from the bulk states. For sample $S3$, e.g. the magnitude of magnetoresistance $[\rho_{xx}(H)/\rho_{xx}(0)-1]$ is ~ 12 at 14 T, almost 8 times higher than that in nonmetallic Bi_2Te_3 [24]. Although the 2D conductance $G^{sp}_{xx} = g_i(e^2/h)k_F l$ accounts for $\sim 10\%$ of the total conductance, the fast-rising bulk magnetoresistance can easily mask any small signals resulting from the surface states, making the detection of surface oscillations much more challenging.

To extract the period of the oscillations, we plot the Landau fan diagram [Fig. 4(c)] using the extrema of $d\rho_{xx}/dH$ and $d\rho_{yx}/dH$ for sample $S3$, as shown in Fig. 4(c). It can be seen that all the data lie on a straight line that intersects the ν-axis at 0.15, suggesting a conventional Schrödinger spectrum. The slope of the extrapolated straight line gives $S_F = 36.0$ T, with an average Fermi wave vector $k_F = 0.033$ Å^{-1}. These values are in good agreement with the parameters of the p-type surface state extracted from the Hall anomaly analysis (Table I).

By fitting the T-dependence of the Hall conductivity amplitudes to the standard Lifshitz-Kosevich expression [Fig. 4(d)], we get the cyclotron mass $m_{cyc} = 0.35m_e$ in sample $S3$ (m_e is the free electron mass). However, due to the limited oscillation periods, the carrier mobility cannot be extracted from the SdH oscillation. With $k_F = 0.033$ Å^{-1}, the average Fermi velocity ($v_F = \hbar k_F/m_{cyc}$) is found to be 1.1×10^5 m/s. This number is more close to the ARPES observed average value of 2.5×10^5 m/s for the holelike surface band ($v_F \sim 0.76$ and 4.3×10^5 m/s along the k_x and k_y directions, respectively) than 3.7 and 4.9×10^5 m/s for the electronlike surface bands surrounding the $\overline{\Gamma}$ and $\overline{\mathrm{M}}$ points, respectively [15]. This fact together with the Hall anomaly analysis suggest that the observed quantum oscillations are most likely coming from the p-type surface state. For the n-type surface states, due to the small Fermi pockets [Fig. 1(a)], their SdH oscillations cannot be clearly resolved.

Interestingly, despite the strong alloying in $Bi_{0.91}Sb_{0.09}$, the magnitude of its surface mobility is the highest ever reported in bismuth-based topological insulators. Compared with Bi_2Te_3 that has a surface to bulk mobility ratio $\mu_s/\mu_b = 12$ at 0.3 K [24], this ratio is ~ 5 for the p-type surface state in $Bi_{0.91}Sb_{0.09}$. These phenomena may be indicative of the unique characteristic of surface states in a topological insulator, in which backscattering caused by atomic scale disorder is absent between states of opposite spin.

In conclusion, we have identified the holelike surface conduction in $Bi_{0.91}Sb_{0.09}$ (111) from weak-field Hall anomaly and SdH oscillations. This surface band exhibits a mobility $\mu_s = 23\,000$-$85\,000$ cm^2/V s, much higher than the bulk value $\mu_b = 9000$-$13\,000$ cm^2/V s. Our observation is consistent with the recent STM studies on $Bi_{1-x}Sb_x$, demonstrating that surface states in $Bi_{1-x}Sb_x$ intend to tolerate disorder resulted from random alloying [19]. These spin-polarized surface states are therefore potentially useful for the future spin-based applications that rely on high carrier mobility.

We would like to thank H.-J. Zhang and S.-C. Zhang for helpful discussion. The high magnetic field measurements were performed at the National High Magnetic Field Laboratory, Tallahassee, Florida. This work was supported by LDRD (12-ERD-027) from Lawrence Livermore National Laboratory. Prepared by LLNL under Contract DE-AC52-07NA27344.

[1] Ph. Hofmann, Prog. Surf. Sci. **81**, 191 (2006).
[2] C. R. Ast and H. Höchst, Phys. Rev. Lett. **87**, 177602 (2001).
[3] T. Hirahara, T. Nagao, I. Matsuda, G. Bihlmayer, E. V. chulkov, Y. M. Koroteev, P. M. Echenique, M. Saito, and S. Hasegawa, Phys. Rev. Lett. **97**, 146803 (2006).
[4] C. R. Ast, J. Henk, A. ernst, L. Moreschini, M. C. Falub, D. Pacilé, P. Bruno, K. Kern, and M. Grioni, Phys. Rev. Lett. **98**, 186807 (2007).
[5] I. Gierz, T. Suzuki, E. Frantzeskakis, S. Pons, S. Ostanin, A. Ernst, J. Henk, M. grioni, K. Kern, and C. R. Ast, Phys. Rev. Lett. **103**, 046803 (2009).
[6] K. Ishizaka *et al.*, Nature Mate. **10**, 521 (2011).
[7] C. L. Kane and E. J. Mele, Phys. Rev. Lett. **95**, 146802 (2005).
[8] B. A. Bernevig and S.-C. Zhang, Phys. Rev. Lett. **96**, 106802 (2006).
[9] J. E. Moore and L. Balents, Phys. Rev. B **75**, 121306 (R) (2007).
[10] L. Fu and C. L. Kane, Phys. Rev. B **76**, 045302 (2007).
[11] J. C. Y. Teo, L. Fu, and C. L. Kane, Phys. Rev. B **78**, 045426 (2008).
[12] H.-J. Zhang, C.-X. Liu, X.-L. Qi, X.-Y. Deng, X. Dai, S.-C. Zhang, and Z. Fang, Phys. Rev. B **80**, 085307 (2009).
[13] M. Z. Hasan and C. L. Kane, Rev. Mod. Phys. **82**, 3045 (2010).
[14] X.-L. Qi and S.-C. Zhang, Rev. Mod. Phys. **83**, 1057 (2011).
[15] D. Hsieh, D. Qian, L. Wray, Y. Xia, Y. S. Hor, R. J. Cava, and M. Z. Hasan, Nature (London) **452**, 970 (2008).
[16] H. Guo *et al.*, Phys. Rev. B **83**, 201104(R) (2011).
[17] D. Hsieh *et al.*, Science **323**, 919 (2009).
[18] A. Nishide, A. A. Taskin, Y. Takeichi, T. Okuda, A. Kakizaki, T. Hirahara, K. Nakatsuji, F. Komori, Y. Ando, and I. Matsuda, Phys. Rev. B **81**, 041309(R) (2010).
[19] P. Roushan, J. Seo, C. V. Parker, Y. S. Hor, D. Hsieh, D. Qian, A. Richardella, M. Z. Hasan, R. J. Cava, and A. Yazdani, Nature (London) **460**, 1106 (2009).
[20] A. A. Taskin and Y. Ando, Phys. Rev. B **80**, 085303 (2009).
[21] A. A. Taskin, K. Segawa, and Y. Ando, Phys. Rev. B **82**, 121302(R) (2010).
[22] A. A. Schafgans, K. W. Post, A. A. Taskin, Y. Ando, X.-L. Qi, B. C. Chapler, and D. N. Basov, Phys. Rev. B **85**, 195440 (2012).
[23] Y. S. Hor and R. J. Cava, J. Alloys Compd. **479**, 368 (2009).
[24] D.-X. Qu, Y. S. Hor, J. Xiong, R. J. Cava, and N. P. Ong, Science **329**, 821 (2010).